Srđan M. Bošnjak

Full Professor
University of Belgrade
Faculty of Mechanical Engineering

Nebojša B. Gnjatović

Teaching Assistant
University of Belgrade
Faculty of Mechanical Engineering

The Influence of Geometric Configuration on Response of the Bucket Wheel Excavator Superstructure

The planar response of the bucket wheel excavator superstructure is investigated by using a four degrees-of-freedom discrete dynamic model where truss-like substructures are employed to model the pillar with counterweight arm and bucket wheel boom. Excitation is due to the resistance-to-excavation. Four representative geometric configurations of the excavator are examined. The fundamental frequency of the system is most sensitive to the change of the geometric configuration, while the fourth mode frequency is the least sensitive. The maximum displacements and accelerations are observed when the bucket wheel boom is in its lowest position.

Keywords: bucket wheel excavator, vibrations, resistance-to-excavation, superstructure response

1. INTRODUCTION

The movement of earth is an intrinsic part of the mining and construction industry. The increasing competition and cost of inputs motivate the need to improve productivity and efficiency, while maintaining high safety standard. Rising demand in the last decades has encouraged the production and use of larger, heavier and more efficient earthmovers, such as the bucket wheel excavator (BWE), [1] and [2]. Unfortunately, the progress in the improvement of the performance of BWE, especially their capacities, has not been equally followed by improvements in the analytical or computational methods. A good proof of this statement are relatively frequent failures of BWE [3] to [10].

The current engineering codes and national standards used in calculations ignore the dynamic external load caused by resistance-to-excavation which is both significant and periodical. For example, the DIN 22261 standard considers dynamic effects by the introduction of the so called equivalent loads. The intensity of the load is defined as the product of the static load and corresponding amplifying dynamic coefficient. While this leads to increased load intensity, the load is still deemed static. The analysis of the dynamic behavior of BWE is important in order to prevent the occurrence of resonance in the system, to create a basis to better analyze stress states in the structural elements of the system, and to facilitate the determination of lifetime of the excavator.

The literature on the research on the dynamics of BWEs is relatively sparse. A review of papers dealing with various issues encountered in the modeling of BWE structure and external loads caused by the resistance-to-excavation is presented in [11] and [12].

The papers [13] and [14] discuss stability problem in the motion of the BWE excavating unit for the single mass oscillatory system, while papers [15] to [17] are dedicated to the problems of determination and measurements of natural frequencies of the bucket wheel excavators' structures as well as their vibrations during mining process.

This paper deals with the BWE SchRs 1760, whose geometric configuration is shown in Fig. 1. The goal of the presented study is to investigate modal characteristics and dynamic response of the superstructure to excitation from the resistance-to-excavation. Participation of the system bending vibrations in horizontal plane, as well as torsional vibrations of the bucket wheel boom structure, in analyzed natural modes is practically insignificant, which allows for precise-enough description of the system dynamic behavior from an engineering accuracy point of view, by assuming that motion is constrained to the vertical plane. The employed approach is twofold. First, a model is developed to represent the external load induced by the resistance-to-excavation. Second, by reducing the vibrations of the bucket wheel excavator superstructure, an extremely complex system of coupled elastic bodies, to vibrations of the system with just four representative degrees of freedom (DOF), it is possible to adequately analyze the dynamic behavior of all of its relevant substructures.

The developed models of excitation and BWE superstructure as well as obtained results were also used as basis for further research presented in [18].

2. MATHEMATICAL FORMULATION

2.1 Modeling the loads induced by the resistance-to-excavation

The external loads induced by the resistance-to-excavation are determined via the use of a model that encompasses all relevant structural parameters and the duty cycle parameters that are essential for the analysis
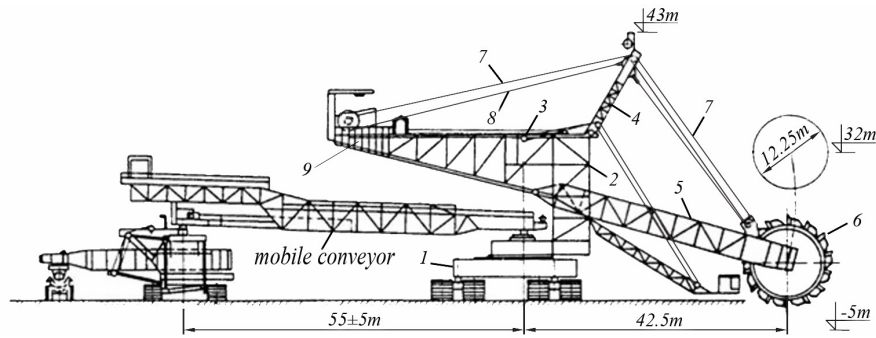
Figure 1. Structural scheme of BWE Sch Rs 1760 / 5 x 32 with mobile conveyor: (1) lower structure with mechanism of transport crawler (vehicular base with caterpillar track), (2) pillar, (3) counterweight arm, (4) portal, (5) bucket wheel boom (BWB), (6) bucket wheel (BW), (7) mechanism comprising rope system for BWB hanging, (8) portal tie-rods (PTR), (9) counterweight

of the kinematics, cutting geometry, and defining external load of BW and BWB. A detailed presentation of the procedure is given in [12], and its validation, using the ideas expounded by Murray-Smith [19], is found in [3] and [20].

The load due to the resistance-to-excavation, Fig. 2, is defined for the case where the pit face height (h_E) is equal to the radius of the BW (r_{BW}=6.125 m). By moving the tangential (R_{Ti}) and normal (R_{Ni}) components of the resistance-to-excavation to point G (the center of gravity of BW and drive unit) and using the in-house developed software RADBAG [3] and [20], the components of the principal force and moment vectors are computed and plotted in Fig. 3.

The profiles of the forces and moments indicate the satisfaction of Dirichlet conditions and so they are expandable via Fourier series as

$$f(t) = \frac{1}{2}(f_{max} + f_{min}) - \frac{f_{max} - f_{min}}{\pi} \sum_n \frac{1}{n} \sin(n\Omega t) \quad (1)$$

where $f \in \{F_V, F_H, M\}$.

The excitation fundamental circular frequency is given as

$$\Omega_1 = 2\pi \left(\frac{n_{BW} n_B}{60} \right), \quad (2)$$

where n_{BW}=4.16 rev/min is the number of revolutions per minute of the BW and n_B=14 is the number of buckets on the BW.
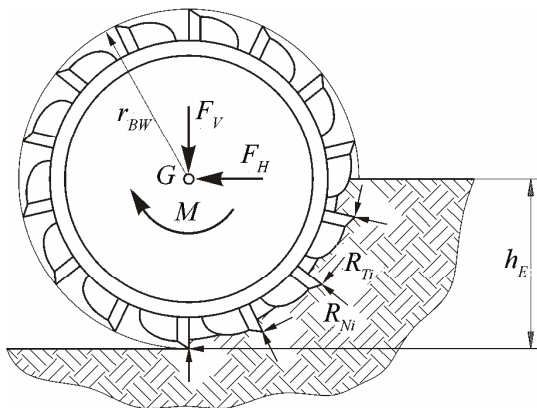

Figure 2. The loads on buckets and the BW caused by the resistance-to-excavation

2.2 Dynamic model of the superstructure

The pillar with counterweight arm (PA) (Fig. 4a) and the BWB (Fig. 4b) are the most dominant of the structural elements of the superstructure in low frequency vibrations. This is attributable to their relatively small stiffness in comparison to that of the portal and the slewing platform. It is worth observing that [11] and [20] provide a detailed procedure to reduce the continuum model of the super–structure to a discrete model of finite degrees of freedom.
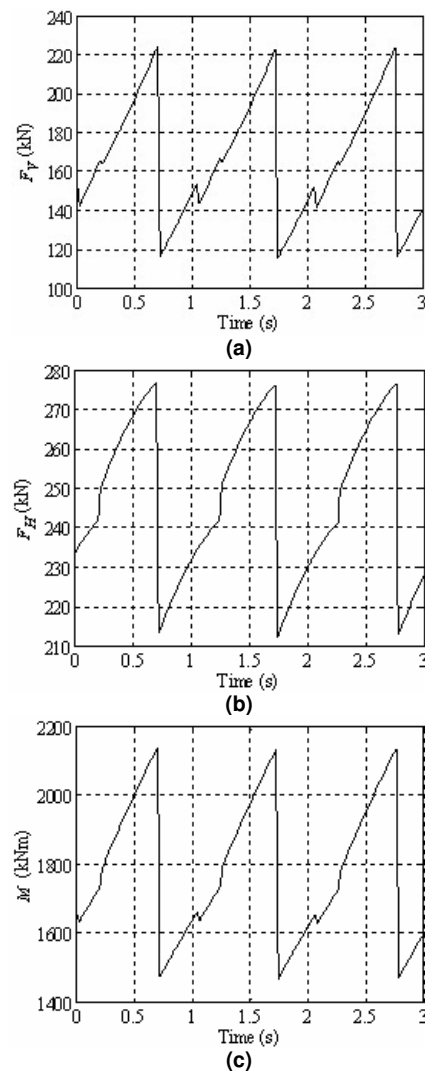

Figure 3. Components of the external non-potential loads caused by the resistance-to-excavation: (a) vertical force, (b) horizontal force, (c) moment

Note that the mixed inertia coefficients of the model shown in Fig. 4a are equal to zero [11]. The potential energy is defined by using Clapeyron's theorem and expressed as

$$U_{PA} = \frac{1}{2}[q_1 \quad q_2][\delta_{PA}]^{-1}[q_1 \quad q_2]^T = $$
$$= \frac{1}{2}[q_1 \quad q_2][k_{PA}][q_1 \quad q_2]^T \qquad (3)$$

where the elements of the flexibility matrix $[\delta_{PA}]$ are defined based on the response of the FEM model to a unit force applied on nodes 84 and 23.

The flexural vibrations of the BWB in the vertical plane are described by generalized coordinate q_4, which measures the perpendicular displacement of the BW center of gravity with respect to the longitudinal axis of the boom, Fig. 4b. The potential energy of the BWB is defined analogously to that of the PA as

$$U_{BWB} = \frac{1}{2}\frac{1}{\delta_{44}}q_4^2 = \frac{1}{2}k_{44}q_4^2. \qquad (4)$$
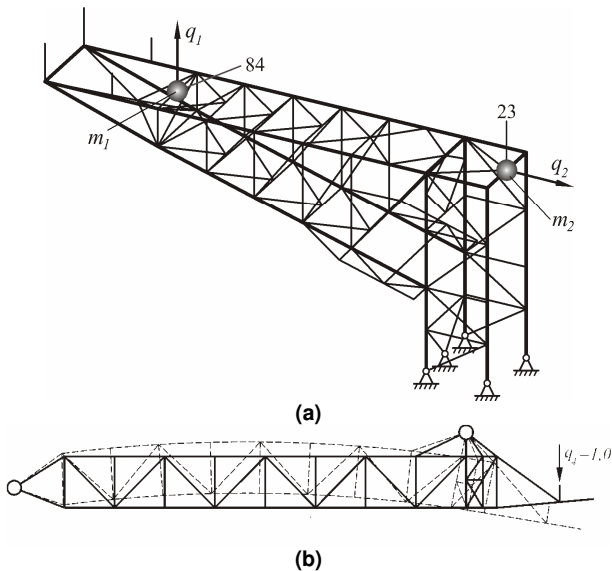

(a)

(b)

Figure 4. (a) Two DOF model of the PA, (b) Single DOF model of the BWB

The dynamic model of the superstructure is finally set up as illustrated in Fig. 5 with the following assumptions: (1) the influence of the portal and lower structure which includes the mechanisms for motion are negligible during low frequency vibrations because of their high stiffness when compared to the stiffnesses of the other structural components; (2) the Young's modulus of the ropes (PTR and the system for hanging the BWB) are linear and load independent; (3) the ropes are massless flexible elements (their masses are reduced in the corresponding nodes of the model); and (4) the soil is undeformable.

In summary, the vibrations of the dynamic model around the position of stable equilibrium are described by four generalized coordinates: q_1- the absolute displacement of the counterweight center of gravity, q_2 - the absolute horizontal displacement of the pillar apex, q_3 - the displacement of the point where the ropes of the hanging system are attached to BWB, perpendicular to the axial axis of the boom, and q_4 - the displacement of the center of gravity of the BW with drive unit, perpendicular to axial axis of the BWB.

2.3 Governing equations of motion

The governing equations are derived on the assumption that the vibrations of the system around the position of stable equilibrium are sufficiently small that the geometric angles α, α_1, α_2, β and γ, depicted in Fig. 5, remain constant.

The displacement of an arbitrary point on the i-th segment in the FEM response with a generalized coordinate $q_4=1.0$ is obtained from an enlarged portion of Fig. 4b, which is depicted in Fig. 6. The displacement function for the segment can be written as

$$y_i(x) = y_i(x)\big|_{q4=1,0} = y_{i,x} = $$
$$= \frac{y_{i+1} - y_i}{x_{i+1} - x_i}x + \frac{y_i x_{i+1} - y_{i+1}x_i}{x_{i+1} - x_i} = k_i x + n_i \qquad (5)$$

where x_i and x_{i+1} are coordinates of the start and end nodes of the segment, while y_i and y_{i+1} are their respective displacements measured in the direction of generalized coordinate q_4. Therefore, the corresponding displacement of an arbitrary point K on the i-th segment (see Fig. 6) for a given value of the generalized coordinate q_4 is $y = y_{i,x}q_4 = (k_i x + n_i)q_4$, and its velocity is $\dot{y} = y_{i,x}\dot{q}_4 = (k_i x + n_i)\dot{q}_4$, where the overdot denotes derivative with respect to time.
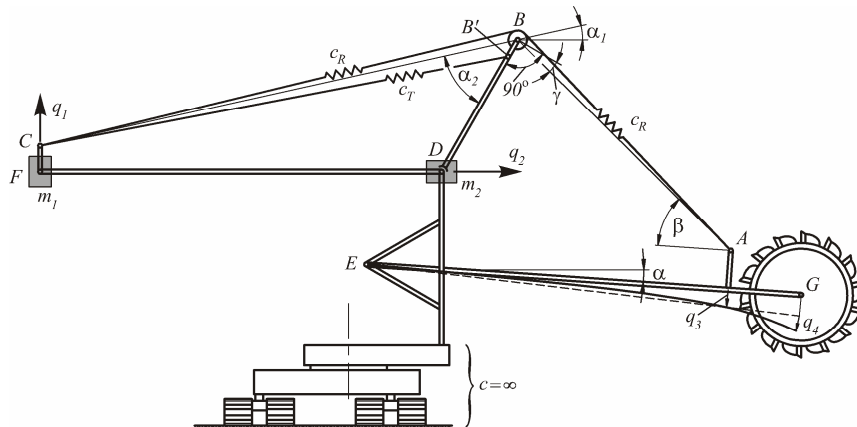

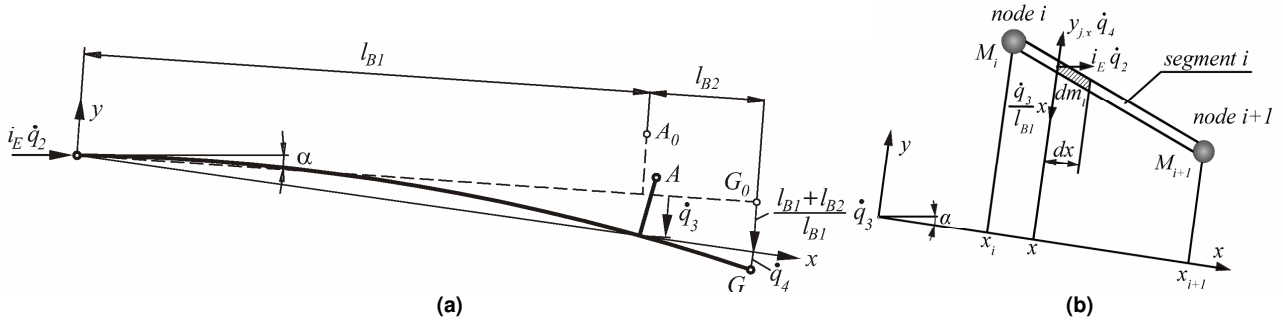**Figure 5. A planar discrete dynamic model for the superstructure**

Figure 7. (a) Plan of BWB velocities, (b) Velocities of the elemental mass of the *i*-th segment
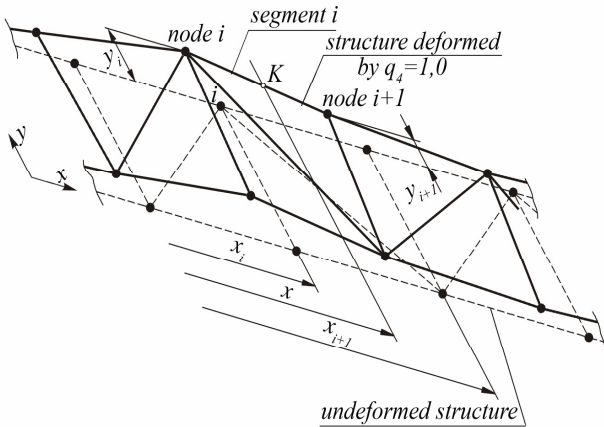

Figure 6. Local linearization of dynamic deflection line of BWB chord

The overall velocity of the arbitrary point is a superposition of that due to the motion of the BWB supports (i.e., points E and A) and that due to the velocity of the generalized velocity $\dot{q}_4$. If the displacement of the hinge E in response to a unit displacement of generalized coordinate q_2 is denoted by i_E, then the velocity of the hinge is $i_E\dot{q}_2$. Using Fig. 7, the absolute velocity of the arbitrary point on the *i*-th segment of the chord $v_{i,x}$ can be inferred and its square can be written as

$$v_{i,x}^2 = \left[i_E\dot{q}_2 + \left(\frac{\dot{q}_3}{l_{B1}}x - y_{i,x}\dot{q}_4\right)\cos\left(\frac{\pi}{2}+\alpha\right)\right]^2 +$$

$$+\left[\left(\frac{\dot{q}_3}{l_{B1}}x - y_{i,x}\dot{q}_4\right)\sin\left(\frac{\pi}{2}+\alpha\right)\right]^2 =$$

$$= i_E^2\dot{q}_2^2 + \frac{1}{l_{B1}^2}x^2\dot{q}_3^2 + y_{i,x}^2\dot{q}_4^2 - \frac{2i_E}{l_{B1}}x(\sin\alpha)\dot{q}_2\dot{q}_3 +$$

$$+2i_E y_{i,x}(\sin\alpha)\dot{q}_2\dot{q}_4 - \frac{2}{l_{B1}}xy_{i,x}\dot{q}_3\dot{q}_4. \qquad (6)$$

The kinetic energy of the *j*-th BWB chord $T_{ch,j}$ is the sum of the kinetic energies of the segments and those of the concentrated masses M_i. The total number of segments is denoted by n_s and each has a mass per unit length which is denoted by m_i. The total number of concentrated masses M_i is denoted by n_{cm} and they represent the masses of the truss webs, devices and equipment located on the boom, belt conveyor, conveyed material, pulleys and a portion of the mass of ropes for boom lifting. Hence,

$$T_{ch,j} = \frac{1}{2}\sum_{i=1}^{n_s}\int_{x_i}^{x_{i+1}} v_{i,x}^2 dm_i + \frac{1}{2}\sum_{i=1}^{n_{cm}} M_i v_i^2 =$$

$$= \frac{1}{2}\sum_{i=1}^{n_s} m_i \int_{x_i}^{x_{i+1}} v_{i,x}^2 dx + \frac{1}{2}\sum_{i=1}^{n_{cm}} M_i v_i^2, \qquad (7)$$

where $v_i^2 = v_{i,x}^2\big|_{x=xi}$ is the square of the velocity of the concentrated mass at node *i*.

The system kinetic energy is given as

$$T = \sum_{j=1}^{4} T_{ch,j} + \frac{1}{2}m_{BW}v_G^2 + \frac{1}{2}m_1\dot{q}_1^2 + \frac{1}{2}m_2\dot{q}_2^2, \quad (8)$$

where the first term on the right-hand side is the kinetic energy of the entire chords, the second is the kinetic energy of the BW-with-drive-unit whose mass is denoted by m_{BW} and the square of the velocity of its centre of gravity (i.e., point G in Fig. 7) is $v_G^2 = v_{i,x}^2\big|_{x=l_{B1}+l_{B2}}$, and the penultimate and last terms present kinetic energy of the PA.

The extensions of the rope and the tie-rod (Figs. 8 and 9) are given respectively as:

$$\Delta_R = i_B\Delta l_{AB} + \Delta l_{BC}, \quad (a)$$
$$\Delta_T = \Delta l_{BC}, \quad (b) \qquad (9)$$

where

$$\Delta l_{AB} = (i_E - 1)q_2\cos(\alpha+\beta) +$$
$$+q_3\sin\beta + h_1\frac{q_4}{l_{B2}}\cos\beta - p\cos\gamma, \qquad (a)$$

$$\Delta l_{BC} = p\sin\alpha_2 - q_1\sin\alpha_1, \quad (b)$$

$$l_{B'C} \approx l_{BC}, \quad (c) \qquad (10)$$

i_B is the number of lines that connect the tip of portal to the BWB, and p is the displacement of the portal tip (node B, Fig. 9b) which is a consequence of the rotation of the portal around the hinge D. Based on the satisfaction of moment equilibrium conditions around the hinge D, it can be expressed as the linear combination of the generalized coordinates of the system:
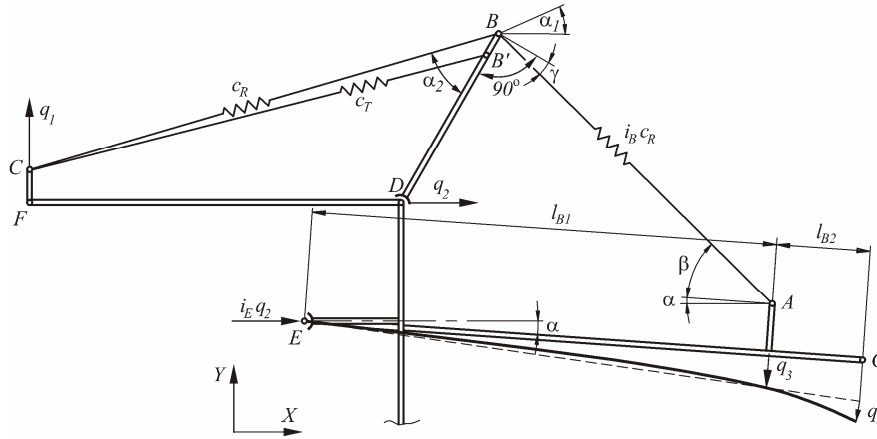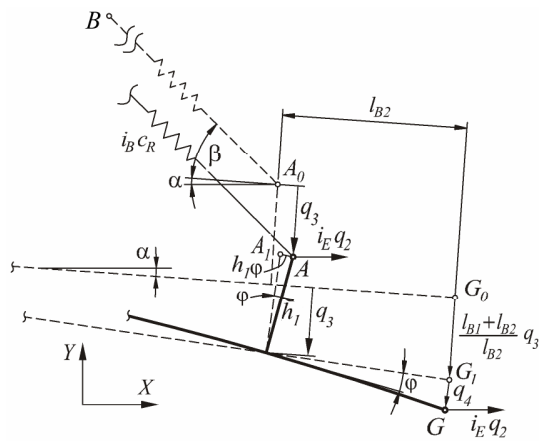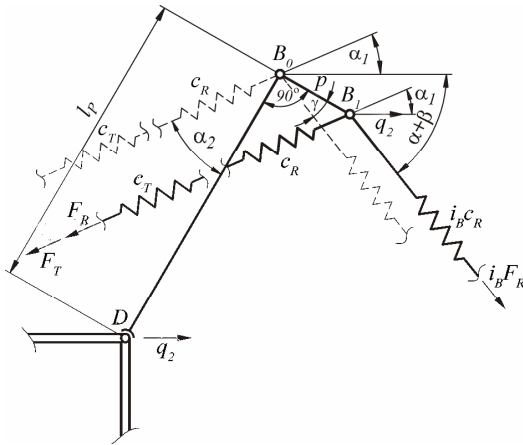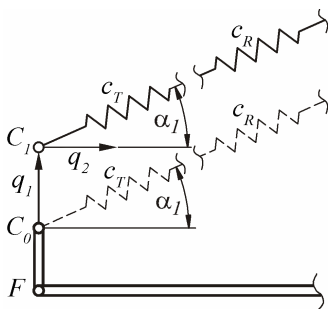
Figure 8. Plan of superstructure displacements

(a)

(b)

(c)

**Figure 9. Displacements of model reference nodes:
(a) nodes A and G, (b) node B, (c) node C**

$$p = \frac{a_1}{e_1}q_1 + \frac{b_1}{e_1}q_2 + \frac{c_1}{e_1}q_3 + \frac{d_1}{e_1}q_4, \quad (11)$$

where

$$a_1 = c_T \sin\alpha_1 \sin\alpha_2 - uc_R \sin\alpha_1, \quad (a)$$

$$b_1 = i_B uc_R(r-1)\cos(\alpha+\beta), \quad (b)$$

$$c_1 = i_B uc_R \sin\beta, \quad (c)$$

$$d_1 = i_B uc_R \frac{h_1}{l_{B2}}\cos\beta, \quad (d)$$

$$e_1 = u^2 c_R + c_T \sin^2\alpha_2, \quad (e)$$

$$u = i_B \cos\gamma - \sin\alpha_2. \quad (f) \quad (12)$$

Substituting Eq. (11) into Eqs. (10) yields

$$\Delta l_{AB} = aq_1 + bq_2 + cq_3 + dq_4, \quad (a)$$

$$\Delta l_{BC} = eq_1 + fq_2 + gq_3 + hq_4, \quad (b) \quad (13)$$

where

$$a = -\frac{a_1}{e_1}\cos\gamma, \quad (a)$$

$$b = (i_B - 1)\cos(\alpha+\beta) - \frac{b_1}{e_1}\cos\gamma, \quad (b)$$

$$c = \sin\beta - \frac{c_1}{e_1}\cos\gamma, \quad (c)$$

$$d = \frac{h_1}{l_{B2}}\cos\beta - \frac{d_1}{e_1}\cos\gamma, \quad (d)$$

$$e = \frac{a_1}{e_1}\sin\alpha_2 - \sin\alpha_1, \quad (e)$$

$$f = \frac{b_1}{e_1}\sin\alpha_2, \quad (f)$$

$$g = \frac{c_1}{e_1}\sin\alpha_2, \quad (g)$$

$$h = \frac{d_1}{e_1}\sin\alpha_2. \quad (h) \quad (14)$$

In view of Eqs. (13), Eqs. (9) can be rewritten as

$$\Delta_R = (i_B a + e)q_1 + (i_B b + f)q_2 + \\ + (i_B c + g)q_3 + (i_B d + h)q_4, \quad (a)$$

$$\Delta_T = eq_1 + fq_2 + gq_3 + hq_4 \ . \quad \text{(b)} \qquad (15)$$

The stiffness of the rope in the system for hanging the BWB c_R and the portal tie-rod c_T are defined as

$$c_{R(T)} = \frac{E_{R(T)} A_{R(T)}}{l_{R(T)}} \ , \qquad (16)$$

where $E_{R(T)}$ is the modulus of elasticity of rope (tie-rod), $A_{R(T)}$ is the cross section of rope (tie-rod), $l_R = i_B l_{AB} + l_{BC} + l_0$ is the total length of rope (with the constant l_0 being the rope length from the tip of the portal to the device which equalizes forces in ropes of two parallel systems of BWB hanging), and $l_T = l_{BC}$ is the tie-rod length.

Noting that there are two identical and parallel systems for hanging the BWB with the device which equalizes forces in the ropes and two identical and parallel PTR, the total potential energy of each subsystem (i.e., ropes and PTR) is given as:

$$U_R = c_R \Delta_R^2 \ , \quad \text{(a)}$$

$$U_T = c_T \Delta_T^2 \ . \quad \text{(b)} \qquad (17)$$

The total potential energy of the system U is simply the sum of the potential energy of the subsystems, and it is written as

$$U = U_{PA} + U_{BWB} + U_R + U_T \ , \qquad (18)$$

Using Fig. 10, the virtual work of non-potential active loads is given as

$$\delta A = -i_E F_H \delta q_2 +$$
$$+ \left(F_V \cos\alpha + F_H \sin\alpha \right) \frac{l_{B1} + l_{B2}}{l_{B1}} \delta q_3 + \qquad (19)$$
$$+ \left(F_V \cos\alpha + F_H \sin\alpha + \frac{M}{l_{B2}} \right) \delta q_4 ,$$

from which the generalized non-potential forces of the system are obtained as

$$Q_1 = 0 \ , \quad \text{(a)}$$

$$Q_2 = -i_E F_H \ , \quad \text{(b)}$$

$$Q_3 = \left(F_V \cos\alpha + F_H \sin\alpha \right) \frac{l_{B1} + l_{B2}}{l_{B1}} \ , \quad \text{(c)}$$

$$Q_4 = F_V \cos\alpha + F_H \sin\alpha + \frac{M}{l_{B2}} \ . \quad \text{(d)} \qquad (20)$$
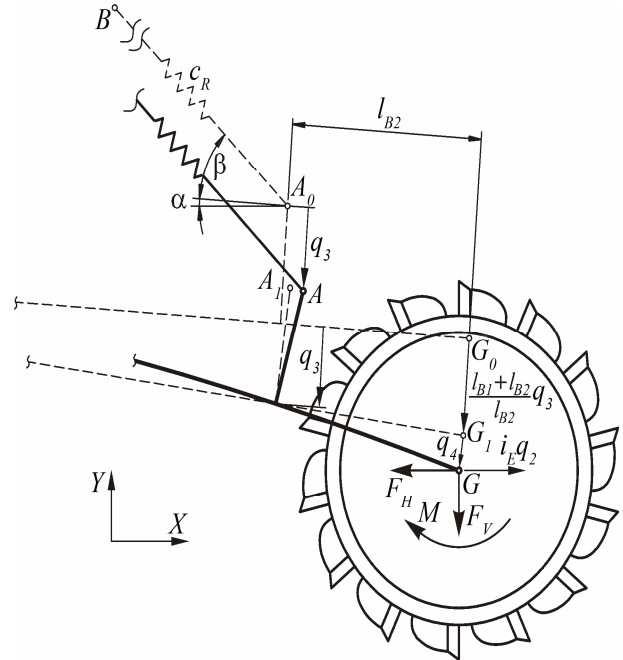
Figure 10. Non-potential loads of the model

In view of forces and moment expressions given in Eq. (1), the vector of generalized non-potential forces is written as

$$\{Q\} = \{Q_0\} + \sum_{n=1}^{\infty} \{Q_n\} \sin\left(n\Omega t\right) , \qquad (21)$$

where

$$\{Q_0\} = \left\{ \begin{array}{c} 0 \\[2mm] -\dfrac{1}{2} i_E \left(F_{H\max} + F_{H\min} \right) \\[3mm] \dfrac{l_{B1} + l_{B2}}{2 l_{B1}} \left[\left(F_{V\max} + F_{V\min} \right) \cos\alpha + \left(F_{H\max} + F_{H\min} \right) \sin\alpha \right] \\[3mm] \dfrac{1}{2} \left[\left(F_{V\max} + F_{V\min} \right) \cos\alpha + \left(F_{H\max} + F_{H\min} \right) \sin\alpha + \dfrac{1}{l_{B2}} \left(M_{\max} + M_{\min} \right) \right] \end{array} \right\} , \qquad (22)$$

$$\{Q_n\} = \left\{ \begin{array}{c} 0 \\[2mm] \dfrac{i_E}{n\pi} \left(F_{H\max} - F_{H\min} \right) \\[3mm] -\dfrac{l_{B1} + l_{B2}}{n\pi l_{B1}} \left[\left(F_{V\max} - F_{V\min} \right) \cos\alpha + \left(F_{H\max} - F_{H\min} \right) \sin\alpha \right] \\[3mm] -\dfrac{1}{n\pi} \left[\left(F_{V\max} - F_{V\min} \right) \cos\alpha + \left(F_{H\max} - F_{H\min} \right) \sin\alpha + \dfrac{M_{\max} - M_{\min}}{l_{B2}} \right] \end{array} \right\} \qquad (23)$$

The application of Lagrange's principle, with the energies (i.e., Eqs. (8) and (18)) and the non-potential force vector, Eq. (21), yields a system of governing differential equations which are symbolically expressed as

$$[m]\{\ddot{q}\} + [k]\{q\} = \{Q\}, \qquad (24)$$

and they describe the system vibrations in the vertical plane.

To permit a detailed analysis of the system beyond the natural frequencies and modal matrices, the following metrics are introduced to measure the participation of the substructures in particular mode shapes:

$$u_{PA} = \frac{U_{PA}}{U}, \quad (a)$$

$$u_{BWB} = \frac{U_{BWB}}{U}, \quad (b)$$

$$u_R = \frac{U_R}{U}, \quad (c)$$

$$u_T = \frac{U_T}{U}. \quad (d) \qquad (25)$$

Attention is given to the forced vibration response because free vibration responses are quickly attenuated in practice due to damping. The particular solution to the governing equations in the out-of-resonance region is assumed as

$$\{q_p\} = \{a_p^{(0)}\} + \sum_{n=1}^{\infty} \{a_p^{(n)}\} \sin(n\Omega t). \qquad (26)$$

This expression is substituted into Eq. (24) to the term its coefficients the use of which permits the expression of the system acceleration and displacement as

$$\{\ddot{q}\} = \{\ddot{q}_p\} =$$
$$= -\sum_{n=1}^{\infty} (n\Omega)^2 \left[R(n\Omega) \right]^{-1} \{Q_n\} \sin(n\Omega t), \qquad (a)$$

$$U_T = c_T \Delta_T^2 \{q\} = \{q_p\} = [k]^{-1}\{Q_0\} +$$
$$+ \sum_{n=1}^{\infty} \left[R(n\Omega) \right]^{-1} \{Q_n\} \sin(n\Omega t), \qquad (b) \quad (27)$$

where $\left[R(n\Omega) \right] = [k] - (n\Omega)^2 [m]$.

The displacement of the BW center of gravity, including drive unit (point G), on the global system reference axis (see Figs. 8 and 9a)

$$p_G = \sqrt{p_{G,X}^2 + p_{G,Y}^2},$$

$$p_{G,X} = i_E q_2 - \frac{l_{B1} + l_{B2}}{l_{B1}} \sin(\alpha) q_3 - \sin(\alpha) q_4, \qquad (28)$$

$$p_{G,Y} = -\frac{l_{B1} + l_{B2}}{l_{B1}} \cos(\alpha) q_3 - \cos(\alpha) q_4,$$

and the magnitude of its acceleration

$$a_G = \sqrt{a_{G,X}^2 + a_{G,Y}^2},$$

$$a_{G,X} = i_E \ddot{q}_2 - \frac{l_{B1} + l_{B2}}{l_{B1}} \sin(\alpha) \ddot{q}_3 - \sin(\alpha) \ddot{q}_4, \qquad (29)$$

$$a_{G,Y} = -\frac{l_{B1} + l_{B2}}{l_{B1}} \cos(\alpha) \ddot{q}_3 - \cos(\alpha) \ddot{q}_4,$$

are the major indicators of the BWE response to the excitation caused by resistance-to-excavation. It is suggested in [21], that the changes to the geometric parameters of chip cross section (thickness and width) due to the system vibrations shall not be greater than the corresponding calculation values by 5 to 7 %. On the other hand, it is suggested in DIN 22261 standard (part 2) that the factor to account for additional dynamic load in vertical direction (Y-axis) of the BWB is ψ_V=0.1. This implies an allowed acceleration value $a_{V,PER}=a_{Y,PER}=0.1g\approx1.0$ m/s^2. The standard ignores additional dynamic load in the X-axis by providing the corresponding factor of additional dynamic factor $\psi_L=\psi_X$=0.

3. NUMERICAL EXAMPLE

The analysis is carried out for the following four typical positions of BWB: Position 1 - BWB is in its highest position (α= –17.7°); Position 2 - BWB is in horizontal position (α=0°); Position 3 - BWB is in "planum" (subgrade level) position (α=15.1°); Position 4 - BWB is in its lowest position (α=22.3°).

The system natural frequencies and the participation of the subsystems in each mode shape are tabulated in Table 1.

The responses of the system to excitation due to resistance-to-excavation for the highest and lowest positions of the BWB are depicted in Figs. 11 and 12. Extreme values and ranges of the generalized coordinates, displacements and accelerations of the point G, for all characteristic positions of BWB, are tabulated in Table 2.

4. DISCUSSION

The following inferences can be deduced from the results presented in Table 1:
(a) In the first mode of vibrations, the influence of the PA is dominant, with the pronounced coupling with PTR. The frequency of the first mode increases with increasing inclination angle of the BWB. Its value in Position 4 is greater than in Position 1 by 8.01 %.
(b) In the second mode, a strong coupling with the PA is observed, and the majority of the potential energy is generated by the PTR. Further, increasing the BWB inclination angle results in decreasing of the second mode frequency. In Position 4, its value is 4.87 % smaller than in Position 1.
(c) The PA is the dominant substructure in the third mode (minimum participation of 88.70 % in Position 1 and a maximum of 95.87 % in Position 3). The change in the third mode frequency due to the changes in the BWB inclination angle is relatively small; its value in

Position 3 is 3.15 % smaller than the value corresponding to Position 1.

(d) The BWB is dominant in the fourth mode as the combined participation of the other subsystems is less than 5%. The fourth mode frequency is practically independent of the BWB inclination angle.

(e) The relatively weak dependence of the natural frequencies spectrum on the system geometry or configuration (BWB positions) supports the adequacy of the selection of the geometric and dynamic parameters of the BWE superstructure.

It is observed that the generalized coordinate q_1 is greatly affected by the fundamental harmonic of excitation with negligible influence from the higher order harmonics.

Table 1. Natural frequencies and participation of the subsystems in percentage ratio

Position	Mode	Frequency	Subsystem			
		Hz	PA	BWB	BWB hanging	PTR
1	1.	0.712	63.75	0.02	5.84	30.39
	2.	1.211	42.01	0.03	9.35	48.61
	3.	4.760	88.70	2.92	1.35	7.03
	4.	5.249	2.88	97.03	0.02	0.07
2	1.	0.745	64.31	0.01	7.73	27.95
	2.	1.197	37.85	0.01	13.47	48.67
	3.	4.645	95.55	0.02	0.96	3.47
	4.	5.231	0.01	99.97	0.01	0.01
3	1.	0.763	62.74	0.03	10.67	26.56
	2.	1.170	37.17	0.06	17.99	44.78
	3.	4.609	95.87	2.21	0.55	1.37
	4.	5.249	2.05	97.69	0.07	0.19
4	1.	0.769	61.25	0.06	12.68	26.01
	2.	1.152	38.05	0.12	20.26	41.57
	3.	4.610	94.63	4.34	0.34	0.69
	4.	5.268	4.10	95.45	0.15	0.30

Table 2. Extreme values and ranges

Notation (unit)	Maximum value				Minimum value				Range			
	Position				Position				Position			
	1	2	3	4	1	2	3	4	1	2	3	4
q_1 (mm)	6.6	11.2	14.2	15.3	-0.9	0.1	0.3	0.2	7.5	11.1	13.9	15.1
q_2 (mm)	2.3	3.1	4.0	4.4	-0.6	0.6	0.6	0.4	2.9	2.5	3.4	4.0
q_3 (mm)	12.1	22.7	30.0	33.0	7.9	17.5	24.3	27.2	4.2	5.2	5.7	5.8
q_4 (mm)	3.8	4.2	4.3	4.2	1.7	1.8	1.8	1.7	2.1	2.4	2.5	2.5
$p_{G,X}$ (mm)	5.8	1.0	-8.1	-13.3	3.7	0.2	-9.0	-14.9	2.1	0.8	0.9	1.6
$p_{G,Y}$ (mm)	-12.0	-24.2	-31.3	-33.2	-16.2	-30.1	-37.5	-39.1	4.2	5.9	6.2	5.9
p_G (mm)	17.1	30.1	38.6	41.9	12.5	24.2	32.3	35.7	4.6	5.9	6.3	6.2
$a_{G,X}$ (m/s^2)	0.25	0.05	0.17	0.24	-0.25	-0.05	-0.17	-0.24	0.5	0.1	0.34	0.48
$a_{G,Y}$ (m/s^2)	0.49	0.55	0.57	0.57	-0.49	-0.55	-0.57	-0.57	0.98	1.1	1.15	1.14
a_G (m/s^2)	0.5	0.55	0.60	0.62	0.0	0.0	0.0	0.0	0.5	0.55	0.60	0.62
q_1 (mm)	6.6	11.2	14.2	15.3	-0.9	0.1	0.3	0.2	7.5	11.1	13.9	15.1
q_2 (mm)	2.3	3.1	4.0	4.4	-0.6	0.6	0.6	0.4	2.9	2.5	3.4	4.0
q_3 (mm)	12.1	22.7	30.0	33.0	7.9	17.5	24.3	27.2	4.2	5.2	5.7	5.8
q_4 (mm)	3.8	4.2	4.3	4.2	1.7	1.8	1.8	1.7	2.1	2.4	2.5	2.5
$p_{G,X}$ (mm)	5.8	1.0	-8.1	-13.3	3.7	0.2	-9.0	-14.9	2.1	0.8	0.9	1.6
$p_{G,Y}$ (mm)	-12.0	-24.2	-31.3	-33.2	-16.2	-30.1	-37.5	-39.1	4.2	5.9	6.2	5.9

Table 3. Relative relations between maximum values and ranges

Notation (unit)	Maximum value				Range			
	Position				Position			
	1	2	3	4	1	2	3	4
q_1 (mm)	1.00	1.70	2.15	2.32	1.00	1.48	1.85	2.01
q_2 (mm)	1.00	1.35	1.74	1.91	1.00	0.86	1.17	1.38
q_3 (mm)	1.00	1.88	2.48	2.73	1.00	1.24	1.36	1.38
q_4 (mm)	1.00	1.11	1.13	1.11	1.00	1.14	1.19	1.19
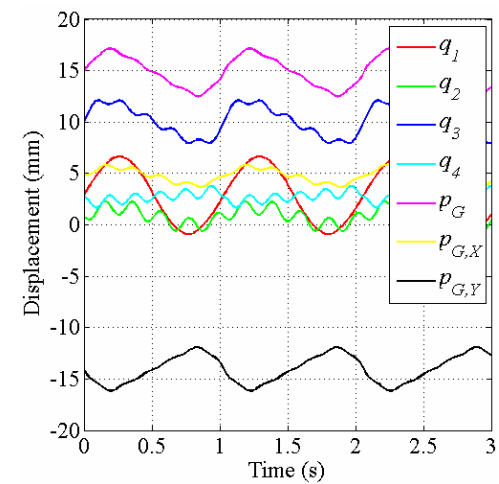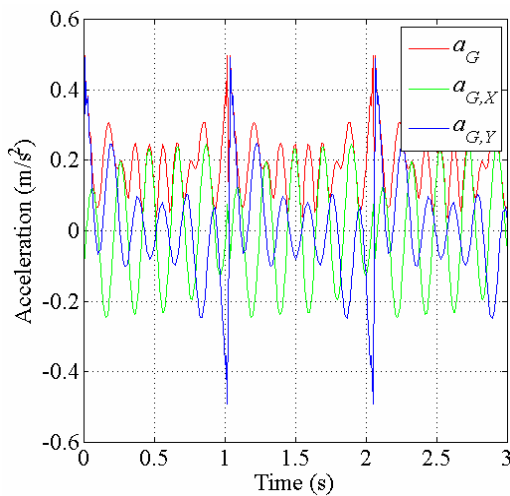
Figure 11. System response in Position 1: (a) generalized coordinates and displacement of point G; (b) acceleration of point G
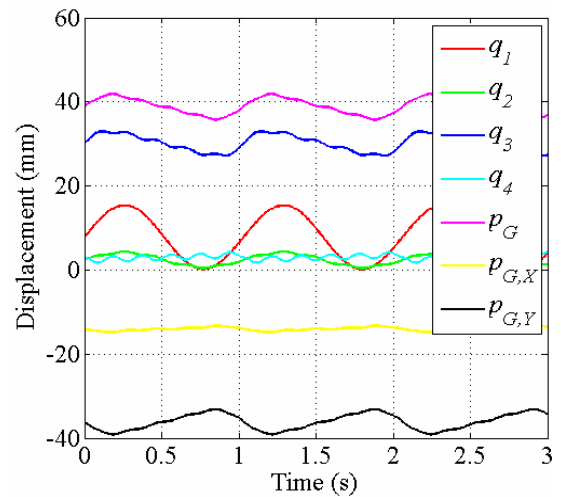

Figure 12. System response in Position 4: (a) generalized coordinates and displacement of point G; (b) acceleration of point G
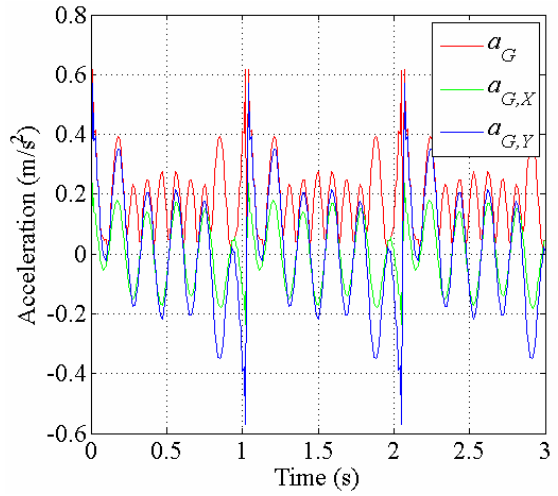
The frequency of the fundamental oscillation of generalized coordinates q_2 and q_3 and corresponds to the frequency of the fundamental excitation harmonic. Further, the response plots show secondary changes whose frequency corresponds to the frequency of the fifth excitation harmonic. In the plots of generalized coordinate q_4, it is noticed that in addition to the fundamental excitation harmonic, which causes the fundamental oscillation, there are notable influences of the fifth and the sixth excitation harmonics.

The maximum values and range of the generalized coordinates change with the changes to the BWB inclination angle from $\alpha = -17.7°$ (at Position 1) up to $\alpha = 22.3°$ (at Position 4). Taking the results at Position 1 as basis for comparison, then the relative relations can be computed and tabulated as in Table 3. An examination of the maximum values shows that the generalized coordinate q_3 is the most sensitive to the geometric configuration change (its maximum value in Position 4 is 2.73 times that in Position 1).

The least sensitive is the generalized coordinate q_4 which has a maximum value in Position 3 that is 1.13 times that in Position 1. The most pronounced change in range is observed with generalized coordinate q_1 - the value in Position 4 is 2.01 times that in Position 1.

5. CONCLUSION

The following conclusions are inferred from the presented analysis:

-The PA is dominant in the first mode of vibration, with significant participation of PTR;

-The majority of the potential energy is accumulated in the PTR in the second mode;

-The PA is overally dominant in the third mode, accounting for a minimum of 88.7% of the total energy;

-The energy accumulated by the BWB, more than 95% of the total energy, is greatest in the fourth mode;

-The fundamental frequency of the system is most sensitive to the change of the geometric configuration, while the fourth mode frequency is the least sensitive;

-The observations for the BWB tip are in agreement with the recommended values in the literature;

-The intensity of the acceleration of the BWB tip in the vertical direction is less than the allowed value of 1 m/s2 as given in the standard DIN 22261;

-The intensity of acceleration of the BWB tip in the horizontal direction approaches, in some positions, 50% of the intensity of acceleration in the vertical direction. Note that the standard DIN 22261 assumes that the value is negligible.

REFERENCES

[1] Durst, W. and Vogt, W.: Bucket wheel excavators, Trans Tech Publications, Clausthal-Zellerfeld, 1989.

[2] Singh S.: The State of the art in automation of earthmoving, Aerospace Eng, vol. 10, no. 4, pp. 179-188, 1997.

[3] Bošnjak, S., Petković, Z., Zrnić, N., Simić, G. and Simonović, A.: Cracks, repair and reconstruction of bucket wheel excavator slewing platform, Eng Fail Anal, vol. 16, no. 5, pp. 1631-1642, 2009.

[4] Rusiński, E., Czmochowski, J., Iluk, A. and Kowalczyk, M.: An analysis of the causes of a BWE counterweight boom support fracture, Eng Fail Anal, vol. 17, no. 1, pp. 179-191, 2010.

[5] Rusiński E, Czmochowski J and Pietrusiak D.: Selected problems in designing and constructing surface mining machinery, FME Transactions, vol. 40, no. 4, pp.153-164, 2012.

[6] Savković, M., Gašić, M., Arsić, M. and Petrović, R.: Analysis of the axle fracture of the bucket wheel excavator, Eng Fail Anal, vol. 18, no. 1, pp. 433-441, 2011.

[7] Savković, M., Gašić, M., Petrović, D., Zdravković, N. and Pljakić, R.: Analysis of the drive shaft fracture of the bucket wheel excavator, Eng Fail Anal, vol. 20, pp. 105-117, 2012.

[8] Semolič, B., Jovanović, P., Kovačev, S. and Obradović, V.: Improving Repair Management of Bucket Wheel Excavator SRs1200 by Application of Project Management Concept, Stroj Vestn-J Mech E, vol. 54, no. 7-8, pp. 565-573, 2008.

[9] Ognjanović, M., Ristić, M. and Vasin, S.: BWE traction units failures caused by structural elasticity and gear resonances, Tehnički vjesnik – Technical Gazette, vol. 20, no. 4, pp. 599-604, 2013.

[10] Jovančić, P., Ignjatović, D., Tanasijević, M. and Maneski, T.: Load-bearing steel structure diagnostics on bucket wheel excavator, for the purpose of failure prevention, Eng Fail Anal, vol. 18, no. 4, pp. 1203-1211, 2011.

[11] Bošnjak, S., Oguamanam, D. and Zrnić, N.: On the dynamic modeling of bucket wheel excavators, FME Transactions, vol. 34, no. 4, pp. 221-226, 2006.

[12] Bošnjak, S., Zrnić, N. and Petković, Z.: Bucket wheel excavators and trenchers – computer aided calculations of loads caused by resistance-to-excavation, in: Machine design, University of Novi Sad, Faculty of technical sciences, pp. 121-128, 2008.

[13] Chudnovskii, V. Yu.: Horizontal vibrations of the excavating part of a rotary excavator and their suppression, Journal of Machinery Manufacture and Reliability, vol. 36, no. 3, pp. 224-228, 2007.

[14] Chudnovskii, V. Yu.: Vertical oscillations of the working unit of a bucket-wheel excavator in a pit face and their suppression, Journal of Machinery Manufacture and Reliability, vol. 37, no. 3, pp. 221-227, 2008.

[15] Gottvald, J.: The calculation and measurement of the natural frequencies of the bucket wheel excavator SchRs 1320/4x30, Transport, vol. 25, no. 3, pp. 269-277, 2010.

[16] Rusiński, E., Dragan, S., Moczko, P. and Pietrusiak, D.: Implementation of experimental method of determining modal characteristics of surface mining machinery in the modernization of the excavating unit, Arch Civ Mech Eng, vol. 12, no. 4, pp. 471-476, 2012.

[17] Gottvald, J.: Analysis of Vibrations of Bucket Wheel Excavator SchRs 1320 During Mining Process, FME Transactions, vol. 40, no. 4, pp. 165-170, 2012.

[18] Bošnjak, S., Oguamanam, D. and Zrnić, N.: The influence of constructive parameters on response of bucket wheel excavator superstructure in the out-of-resonance region, Arch Civ Mech Eng, vol. 15, no. 4, pp. 977-986, 2015.

[19] Murray–Smith, D.J.: Methods for External Validation of Continuous System Simulation Model, Mathematical and Computer Modeling of Dynamical Systems, vol. 4, no. 1, pp. 5-31, 1998.

[20] Bošnjak, S., Petković, Z., Zrnić, N. and Petrić, S.: Mathematical modeling of dynamic processes of bucket wheel excavators, Procedings of the 5th MATHMOD, 8-10.02. 2006, Vienna, pp. 1-8

[21] Dombrovskiy, N.: Multi – bucket excavators: theory, construction, calculation (In Russian), Mashinostroenie, Moscow, 1972.

УТИЦАЈ ГЕОМЕТРИЈСКЕ КОНФИГУРАЦИЈЕ НА ОДЗИВ ГОРЊЕ ГРАДЊЕ РОТОРНОГ БАГЕРА

С. М. Бошњак, Н. Б. Гњатовић

У раду је анализиран одзив горње градње роторног багера у вертикалној равни применом редукованог динамичког модела са четири степена слободе. Подструктуре стуба са стрелом противтега и стрела ротора третиране су као просторне решеткасте конструкције. Побуду у динамичком моделу представља отпор копању.

Анализирано је динамичко понашање за четири карактеристичне геометријске конфигурације горње градње и на основу приказаног истраживања може се извести закључак да на основну фреквенцију система геометријска конфигурација има највећи утицауј, док је четврта сопствена фреквенција

најмање осетљива на промену разматраног параметра. Максималне вредности померања и убрзања референтних тачака система јављају се при најнижем положају стреле ротора.